Density-compensated overturning in the Labrador Sea

Sijia Zou[1,4*], M. Susan Lozier[1], Feili Li[1,5], Ryan Abernathey[2] and Laura Jackson[3]

[1]Duke University, Durham, North Carolina, USA; [2]Columbia University/Lamont Doherty Earth Observatory, New York, USA; [3]Met Office, Exeter, UK.

[4]Now at Woods Hole Oceanographic Institution, Woods Hole, Massachusetts, USA.

[5]Now at Georgia Institute of Technology, Atlanta, Georgia, USA.

*Corresponding author: Sijia Zou (szou@whoi.edu)

The Atlantic Meridional Overturning Circulation, a key constituent of the climate system, is projected to slow down in the 21st century due to a weakening of the Labrador Sea convection, itself a response to greenhouse gas warming and/or enhanced freshwater flux from the Arctic. However, the first observations from the Overturning in the Subpolar North Atlantic Program reveal a minimal response of the Meridional Overturning Circulation to the strong Labrador Sea convection during winters of 2015-2016. From an analysis of observational and reanalysis data, we show here that this weak response can be explained by strong density compensation in the Labrador Sea. While convection induces strong changes of temperature and salinity in the basin interior, the export of the thermal and haline anomalies to the boundary current largely takes place along density surfaces. As a result, the transformation across density surfaces, i.e. the imprint on the overturning circulation, is relatively small. This finding highlights the critical relationship between temperature and salinity in determining the overturning strength in the Labrador Sea and underlines the necessity of accurate freshwater flux estimates for improved MOC predictions.

Paleo-oceanographic and modeling studies have consistently linked the Meridional Overturning Circulation (MOC) variability to the strength of Labrador Sea convection[1-3]. However, assessing the importance of convection to the MOC has been stymied by the relatively large uncertainty of the indirect estimates of the diapycnal (i.e. across density surfaces) mass flux in the Labrador Sea (2-10Sv; 1 Sv = $10^6 m^3/s$), which have been based on indirect estimates (see **Supplementary Information**)[4-9].

Recent observational studies have provided new insights into the linkage between Labrador Sea convection and the MOC. The Overturning in the Subpolar North Atlantic Program (OSNAP) has provided the first continuous measurements for the MOC in density space across the Labrador Sea from August 2014 to April 2016[10,11]. With a mean of 3.3 Sv and a monthly standard deviation (SD) of 1.1 Sv, the weak Labrador Sea MOC contributes minimally to the total overturning circulation in the subpolar North Atlantic (14.9Sv; **Fig.1a**). This finding is especially surprising because convection in the Labrador Sea during the 2015/2016 winters, among the largest ever observed[12], was expected to significantly strengthen the MOC. A similarly small MOC in the Labrador Sea (2 Sv) was reported based on a composite of hydrographic sections during 1990-1997, years over which the basin experienced strong wintertime convection[5]. This study further showed that heat transport across the Labrador Sea was accomplished primarily along density surfaces (i.e. by means of the horizontal gyre circulation) with little contribution from the MOC, a partitioning attributed to a large degree of density compensation by temperature and salinity. This work, and the recent OSNAP observations, raise the question as to how density compensation impacts the MOC strength and whether the compensated relationship is persistent with time.

To answer these questions, we use the 21-month continuous observations from OSNAP to analyze the transport and water mass structure along OSNAP West (from the Labrador shelf to the southwestern tip of Greenland; **Fig.1b inset**), and then compare the transformation in density space with that in temperature and salinity space. The analysis is repeated for a longer temporal record using an ocean reanalysis dataset.

Transport and water mass structure along OSNAP West

The Labrador Sea is characterized by strong boundary currents and weak flow in the basin interior[13,14] (**Fig.1b**). Waters enter the basin via the West Greenland Current (WGC) and exit in the Labrador Current (LC). The two boundary currents have similar vertical transport structure, but they carry waters of distinct properties (**Fig.2**). Above the shelf-break, cold and fresh waters (θ<2.0°C, S<34.10) from the Nordic Seas are transported into the basin by the WGC. On the other side of the basin, the LC exports the coldest fresh waters (θ<0.2°C, S<34.00). These waters primarily originate from the Baffin Bay and the Hudson Bay. Seaward of the shelf and below the surface layer (~200-1000m), the WGC carries warmer and saltier Atlantic-origin waters (θ~4.5°C, S~34.94) into the Labrador Sea. As these waters are advected downstream, the instability of the WGC facilitates property exchange with the large reservoir of cold and fresh Labrador Sea Water (LSW), the product of convection, in the basin interior[15,16] (**Fig.2**). Additionally, direct heat loss and freshwater input within the boundary current may also lead to property modification of these waters. As a result, the exiting LC is much colder and fresher compared to the incoming WGC at these intermediate depths.

In the deep layer (below ~1500m), the Overflow Waters (OW), which include the relatively salty Northeast Atlantic Deep Water (NEADW; θ~2.8°C, S~34.92) and the fresh Denmark Strait Overflow Water (DSOW; θ~1.5°C, S~34.90), flow into the basin via the WGC. The properties of these deep waters in the LC are similar to those in the WGC, with slight modifications. The 21-month mean (August 2014 - April 2016) transport of the entire WGC is 41.5 Sv, with a monthly SD of 4.4 Sv. This number roughly equals the total transport of all waters exiting the basin (-43.1 $\pm$ 4.4 Sv), with the difference -1.6 Sv due to the Arctic throughflow from the Davis Strait[17].

Weak volume flux in density space

An accounting of the horizontal transport in each density layer (**Fig.1b)** reveals the weak diapycnal mass flux. Even though large incoming and outgoing transports are observed in each layer, net transports are

quite small. For example, in the upper layer between 27.32 kg/m^3 and 27.70 kg/m^3, the transport of the incoming waters is 11.0±2.4 Sv, of which 7.6±2.3 Sv exits the basin within the same density layer. The resultant net transport, 3.4±1.3 Sv, contributes to diapycnal mass flux by transforming to the LSW layer (assuming that all diapycnal transformation occurs between neighbouring layers). In the LSW layer (27.70-27.80 kg/m^3), the net volume flux is -3.9±1.9 Sv, indicating a net production of the LSW. Since the transformation rate from the upper layer is 3.4 Sv, there must be a small transformation (~0.5 Sv) from the denser layer (i.e. the NEADW layer) into the LSW layer. In the OW layers, net transports of 2.8±1.0 Sv and -1.3±0.5 Sv are observed in the NEADW layer (27.80-27.89 kg/m^3) and in the DSOW layer (>27.89 kg/m^3), respectively. Such a transport structure suggests a possible transformation from NEADW to DSOW within the Labrador Sea. As shown in **Fig.1a**, there is indeed a small overturning cell present in these deep layers.

The weak diapycnal mass flux across OSNAP West is reflected by the small difference in the isopycnal (i.e. density surfaces) slopes that bound the waters of the WGC and the LC. These comparable isopycnal slopes stand in stark contrast to the significant difference in the isotherm and isohaline slopes (**Fig.2a-b**). This contrast indicates strong density compensation by temperature and salinity in the boundary current, which we explore next.

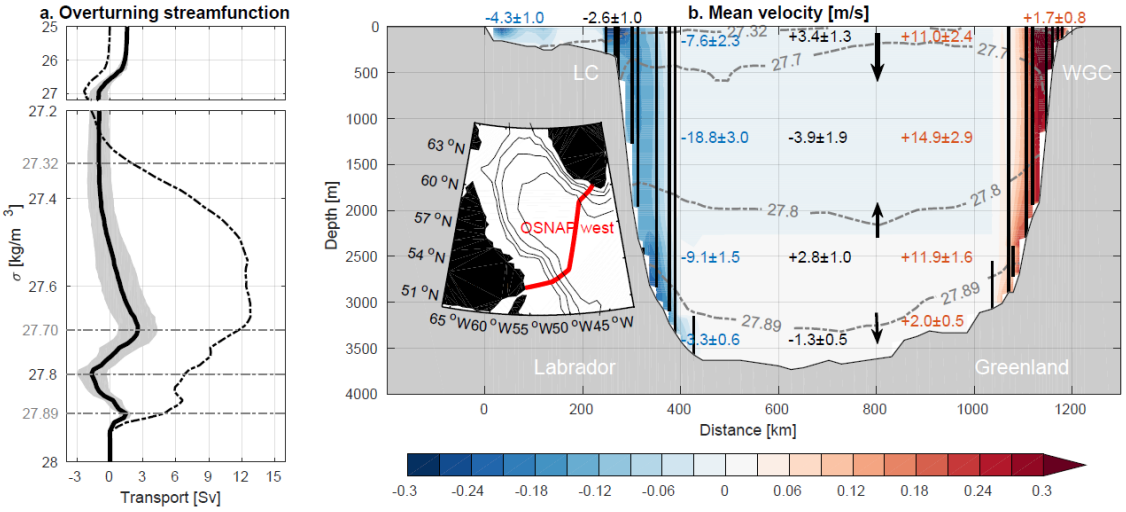

Fig.1: Observed circulation along OSNAP West. (a) The mean overturning streamfunction from August 2014 to April 2016 along OSNAP West (solid black), with its monthly SD shaded in gray. The mean overturning streamfunction along the entire OSNAP line (from Labrador to Scotland) is plotted in dashed black. **(b)** The mean velocity perpendicular to OSNAP West (inset). Positive (negative) velocities indicate flow into (out of) the basin. Black lines show mooring locations and dashed gray contours denote density surfaces. The transport (mean ± monthly SD) of the total inflow (outflow) in each density class is labeled in red (blue), with the net transport labeled in black. Arrows indicate directions of diapycnal transformation. WGC: West Greenland Current; LC: Labrador Current.

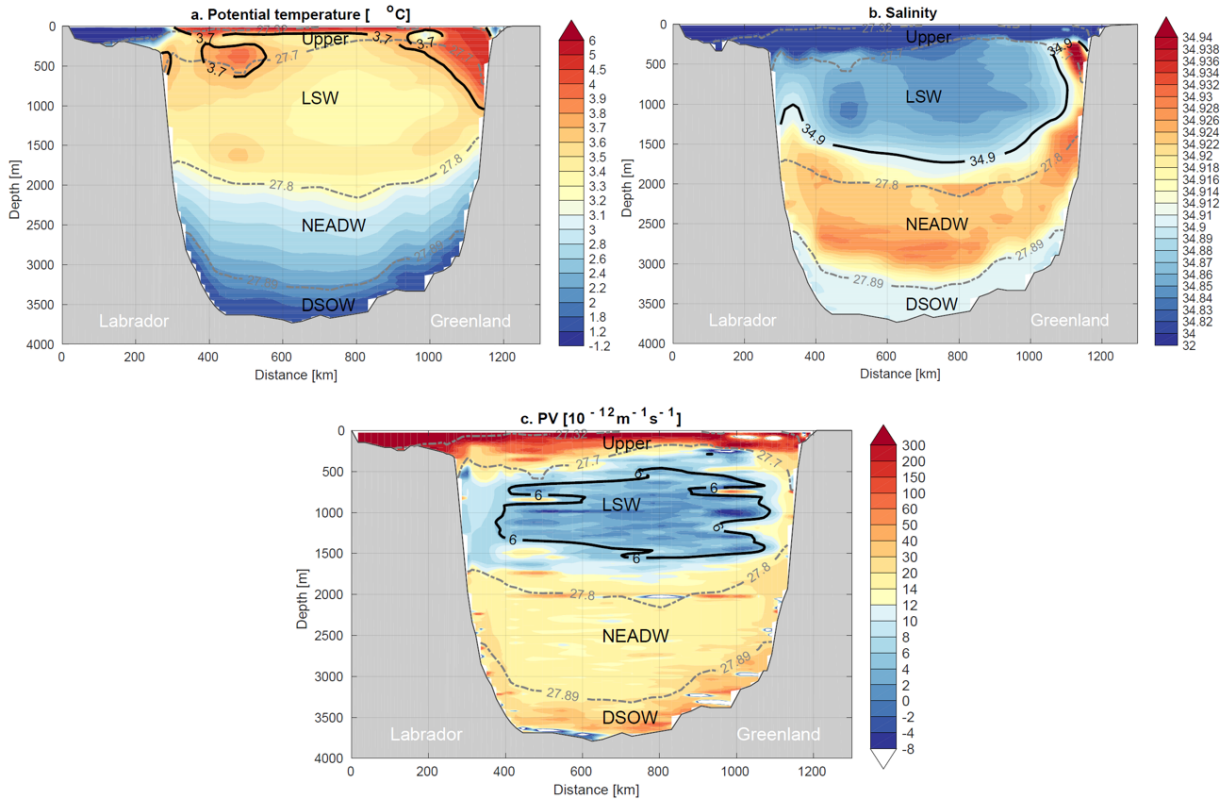

Fig.2: Observed property fields along OSNAP West. (a) The 21-month mean potential temperature. The black contour shows the 3.7°C isotherm, where the maximum overturning in temperature space is reached (**Fig.3b**). **(b)** As in **(a)** except for salinity. Here, the isohaline of 34.90 (where the maximum overturning in salinity space is reached; **Fig.3c**) is contoured in black. **(c)** As in **(a)** except for potential

vorticity. The contoured isopleth of $6\times10^{-12}m^{-1}s^{-1}$ denotes the newly-formed LSW. Densities are plotted in dashed gray. Upper: upper layer; LSW: Labrador Sea Water; NEADW: Northeast Atlantic Deep Water; DSOW: Denmark Strait Overflow Water.

Strong volume flux in temperature-salinity space

To illustrate the impact of density compensation, we grid the mean transports in potential temperature and salinity (θ-S) space (**Fig.3a**). The transport in each θ-S grid represents the total volume flux across the OSNAP West section with shared temperature and salinity (see **Methods**), and is therefore useful in diagnosing water mass transformation in terms of properties. In the upper layer, 9.5±2.4 Sv of the warm and salty incoming waters (transport-weighted mean $\bar{\theta}$~4.7°C, $\bar{S}$~34.84) become colder and fresher ($\bar{\theta}$~3.3°C, $\bar{S}$~34.67) when exiting the basin. Since these thermal and haline changes largely occur along isopycnals, most of these waters (6.0±2.2 Sv) are exported in the same density class. The property changes for the remaining 3.5±1.3 Sv are not density compensated and, as such, are transformed to LSW layer, as discussed above. Similar along-isopycnal transformation of temperature and salinity takes place in the other deep layers: in the LSW layer, the transformation is 12.4±2.8 Sv with significant property changes (from $\bar{\theta}$~3.8°C, $\bar{S}$~34.92 to $\bar{\theta}$~3.4°C, $\bar{S}$~34.87); in the NEADW layer, the transformation is 6.0±1.3 Sv with smaller property changes (from $\bar{\theta}$~2.9°C, $\bar{S}$~34.93 to $\bar{\theta}$~2.8°C, $\bar{S}$~34.92); and the transformation in the DSOW layer is 1.1±0.3 Sv (from $\bar{\theta}$~1.9°C, $\bar{S}$~34.91 to $\bar{\theta}$~1.8°C, $\bar{S}$~34.90).

Collectively these analyses show that, while convection during the OSNAP observational period produced a large transformation of temperature and salinity, a weak diapycnal mass flux (and therefore a weak MOC) resulted because the thermal and haline changes in the boundary current primarily occurred along isopycnals. This finding emphasizes the important role of density compensation in setting the overturning strength in the Labrador Sea. If we consider transformation in temperature and salinity space separately, the resultant "MOC" (by using the term "MOC" in temperature or salinity space, we mean the net transport across isotherms or isohalines) is as large as 13.9 ± 3.0 Sv in temperature space (MOC_θ;

Fig.3b) and 11.4 ± 2.8 Sv in salinity space (MOC_S; **Fig.3c**). Both of these estimates are 3-4 times greater than the MOC in density space. Many models are known to exhibit property biases in the Labrador Sea[18], especially for salinity[19,20] due to large uncertainties in modeling the hydrographic cycle, sea-ice interactions, Greenland ice sheet melting, the freshwater pathways and/or mixing. Such salinity biases may lead to a temperature-dominated density structure across the basin such that the transformation across isopycnals (i.e. the MOC) would resemble the much stronger transformation across isotherms (i.e. MOC_θ) (**Fig.4**). It is also possible that salinity biases change the pattern of convection (by, for example, producing too much deep water and/or producing it in areas outside the observed region[21]) and /or influence the relative proportion of isopycnal and diapycnal mixing between the boundary current and the basin interior. We surmise that in both cases an overestimate of MOC may result, which has the effect of exaggerating the impact of convection[22].

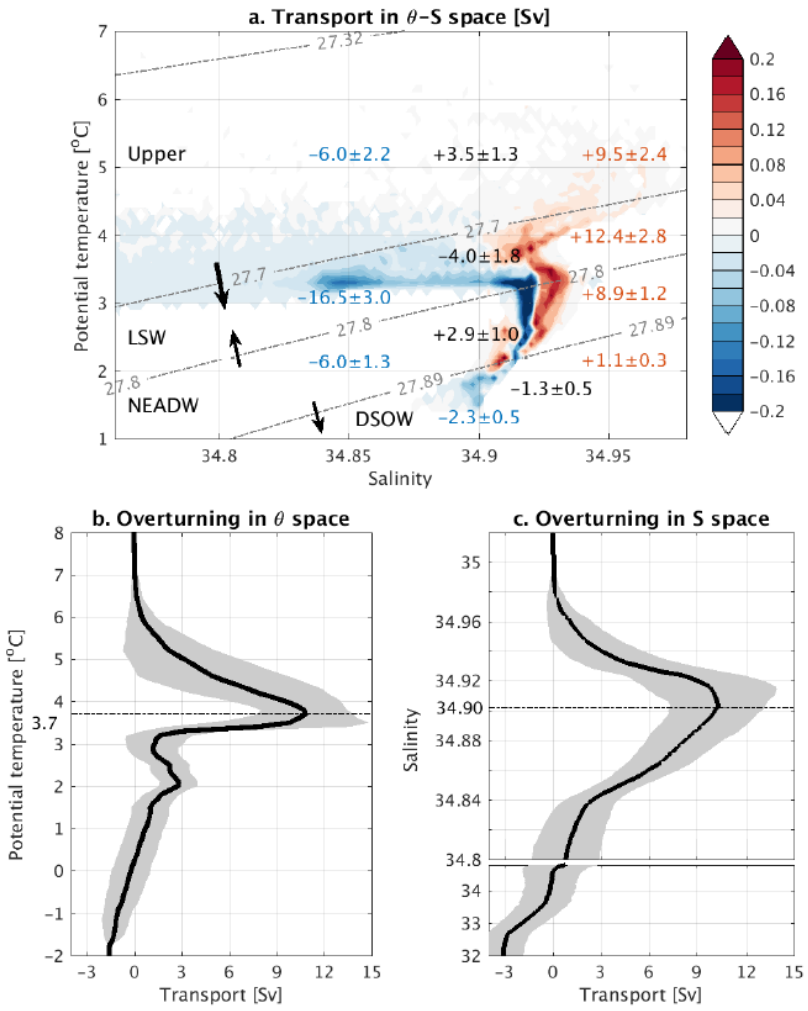

135

136 **Fig.3: Observed transformation in θ-S space. (a)** The 21-month mean volume flux in θ-S space.
137 Positive (negative) transport in each grid box ($\Delta\theta$=0.1°C; $\Delta S = 0.002$) indicates that waters with the
138 same temperature and salinity flow into (out of) the basin. The total positive (negative) transport between
139 density surfaces (mean $\pm$ monthly SD) is labeled in red (blue), with the net transport labeled in black.
140 Arrows indicate directions of diapycnal transformation. **(b)** The overturning streamfunction with respect
141 to temperature space, with a maximum reached at 3.7°C. **(c)** The overturning streamfunction with respect
142 to salinity space, with a maximum reached at 34.90.

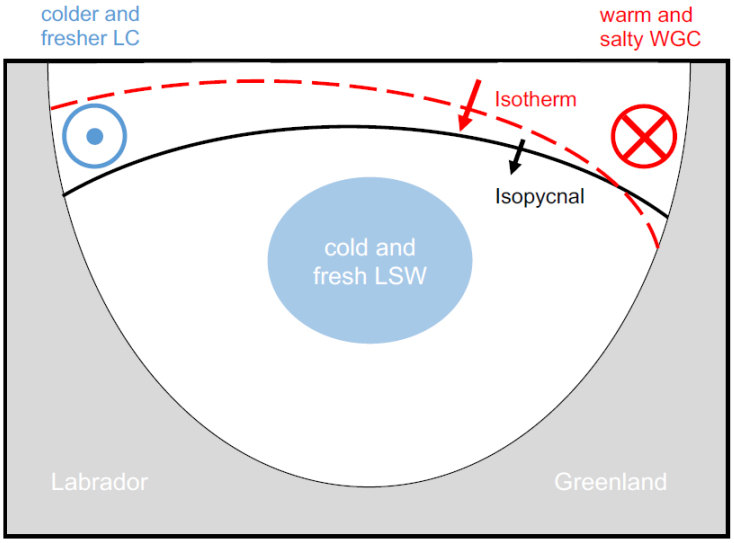

143

144 **Fig.4: A schematic of transformation along OSNAP West.** Warm and salty waters enter the basin via
145 the WGC and exit in the LC with cold and fresh anomalies, a result from the exchange between the
146 boundary current and the cold and fresh basin interior. The resultant sharp tilt of isotherm from the WGC
147 to the LC (red dashed line) suggests strong transformation with respect to temperature space (red arrow).
148 In contrast, the isopycnal slope is comparable on both sides of the basin due to density compensation,
149 resulting in a weak diapycnal transformation (black arrow).

150 Though this 21-month record provides clear evidence for a density-compensated MOC in the Labrador
151 Sea, the relatively short time series begs the question as to the representativeness of this time period. We
152 examine this question by repeating our analysis with an ocean reanalysis dataset GloSea5 that represents
153 well the observed water mass distribution and velocity structure across the Labrador Sea (see **Methods**
154 and Extended Data **Fig.1-3**). The simulated MOC during August 2014-April 2016 is 2.3 ± 1.2 Sv. The
155 mean MOC over the 25-year domain of the reanalysis (1993-2017) is 2.7 Sv with a monthly SD of 2.1 Sv.
156 Interestingly, during the strongest convective period (1993-1996), the MOC is as low as 2.0 Sv. All of
157 these values are comparable to the OSNAP observations, as well as to estimates from hydrographic
158 sections during the 1990s[5]. In addition, the large overturning in temperature space (13.3 ± 5.6 Sv) and in

159 salinity space (17.6 ± 4.7 Sv) from 1993 to 2017 show a consistent picture of strong along-isopycnal
160 mixing between the boundary current and the basin interior. Thus, it is suggested that 1) the minimal
161 contribution of the Labrador Sea convection to the total overturning in the subpolar gyre is likely
162 representative of longer time periods and 2) density compensation of the large temperature and salinity
163 changes is primarily responsible for the disconnect between convection and overturning in this basin.

164 **Temporal variability of the overturning transports**

165 We now turn our attention to the temporal variability of the overturning transports in the Labrador Sea.
166 The observed monthly overturning transports are compared to the amount of newly-formed LSW (i.e. the
167 product of convection) volume across OSNAP West (**Fig.5a**). The volume is characterized as the cross-
168 sectional area (unit: m^2) with low potential vorticity (PV$\leq 6\times10^{-12}m^{-1}s^{-1}$) in **Fig.2c**, the variability of
169 which well represents the variability of the total newly-formed LSW volume within the entire Labrador
170 Sea (i.e. total volume of low PV in the basin; Extended Data **Fig.4**). The maximum LSW volume occurs
171 in April 2015, after which cold and fresh LSW is exported out of the basin via the LC. The cold and fresh
172 anomalies in the LC enhance the cross-sectional temperature and salinity difference and result in
173 increased MOC_θ and MOC_S. While MOC_θ and MOC_S depend on differences in temperature and salinity
174 across the basin, the temporal variability of MOC_θ is more correlated to temperature anomalies in the
175 outgoing LC whereas MOC_S is more correlated to the incoming salinity anomalies in the WGC (Extended
176 Data **Fig.5**).

177 Density compensation results in weak monthly variability of the MOC, with no direct linkage to
178 convection (**Fig.5a**). We note that the observed variability of the diapycnal mass flux along OSNAP West
179 does not reflect the variability of the total diapycnal transformation in the Labrador Sea (i.e. northwest of
180 OSNAP West) because the system is not in steady state. The total diapycnal transformation exhibits much
181 stronger monthly variability in response to surface forcing and diapycnal mixing in the basin interior, and

is mostly damped by volume changes in isopycnal layers[23] (Extended Data **Fig.6**). In short, the LSW production variability does not translate to the MOC variability.

The observed monthly variability of the overturning transport is well simulated in GloSea5 (Extended Data **Fig.7**). Compared to the monthly climatology over the 1993-2017 time period, simulated MOC and MOC_S during the OSNAP period (August 2014 – April 2016) do not stand out. MOC_θ, on the other hand, has a stronger and earlier peak (June compared to October for the long-term mean). This difference is likely attributable to enhanced convection during the OSNAP years, which can lead to colder anomalies exported to the boundary current at a faster rate[24].

On interannual time scales, the volume of newly-formed LSW is correlated with MOC_θ (r=0.54), with the former leading by 1 year (**Fig.5b**). As on monthly time scales in the observational record, the interannual variability of MOC_θ from this modeled time series is related to temperature anomalies in the LC (Extended Data **Fig.8**), which are product of the exchange with the interior. In contrast, no significant correlation is found between LSW volume and MOC_S (r=-0.20). We explain this result by noting that changes in the salinity of the incoming WGC, the freshwater flux from the Arctic and the freshwater cycle can all impact salinity variability and thus MOC_S in the basin. While temperature transformation seems tightly coupled to convective heat loss in the interior, the primary cause of the salinity transformation awaits further investigation. Finally, MOC remains low throughout the time series and shows insignificant correlation (r=0.11) with the LSW volume variability. Such a weak correlation and the persistently low MOC magnitude in the Labrador Sea over the past two decades, which contain periods of both strong and intermediate convections, provide compelling evidence that density compensation explains the minimal imprint of the Labrador Sea convection on the MOC.

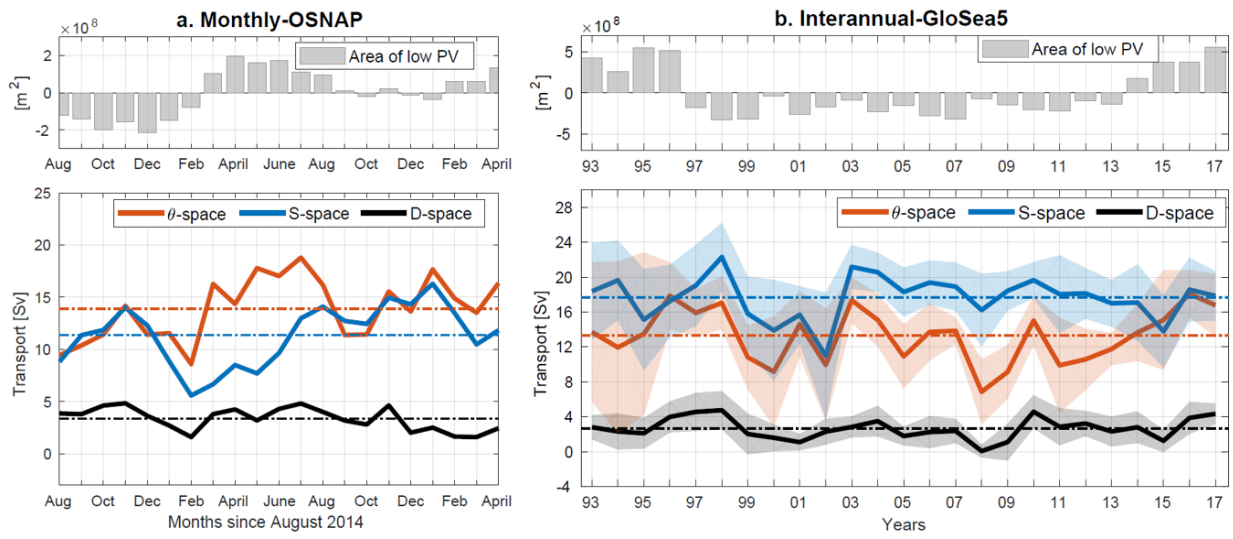

Fig.5: Variability of LSW volume and overturning transports. (**a**) Observed monthly time series of newly-formed LSW volume anomalies (relative to the 21-month mean; gray bars), MOC_θ (orange), MOC_S (blue), and MOC (black) along OSNAP West. Colored dashed lines indicate the 21-month mean of the overturning transports in each coordinate. **(b)** Simulated annual time series of newly-formed LSW volume (gray bars), MOC_θ (orange), MOC_S (blue), and MOC from GloSea5. Color shading indicates the monthly SD for each year. All time series have been detrended. The results based on original (i.e. non-detrended) time series yield similar conclusions.

Discussions and implications

We have presented observational evidence for significant density compensation of the mixing between the boundary current and the basin interior in the Labrador Sea, which serves to diminish the impact of convection on the MOC. This finding highlights the critical relationship between temperature and salinity in setting the density structure, thereby the MOC, in the basin. While global warming and emerging freshwater accumulation from Greenland[25,26] may lead to a weakened convection in the Labrador Sea, it remains unclear whether these changes would break the compensated influence of temperature and salinity on density, and thereby modify the MOC. As such, this work suggests that models need to

219 correctly simulate the salinity (as well as temperature) field in order to adequately reproduce the MOC
220 and predict its response to future climate change.

221 Finally, we note that Lozier et al. (2019)[10] offered a reconciliation between the recent OSNAP results and
222 past studies[3,27] that have used mid-depth densities in the Labrador Sea as proxies for the downstream
223 MOC strength. Specifically, they note that a reconciliation "is possible if the density anomalies in the
224 Labrador Sea are signatures of upstream density anomalies imported from the eastern subpolar gyre
225 and/or have a remote impact on the overturning between Greenland and Scotland." Our work here
226 suggests that the temperature and salinity anomalies formed via convection might also serve as proxies
227 for the same reason, but they are unlikely drivers of the downstream MOC variability. Indeed, a recent
228 estimate of the mean MOC in the subpolar North Atlantic, reconstructed from combined shipboard
229 current measurements and hydrographic profiles, suggest that the Nordic Seas, rather than the Labrador
230 Sea, are "key to the state of the MOC"[28].

231 **Methods**

232 *Observational data across the OSNAP array*

233 We use gridded property and velocity data across the OSNAP West section for each 30-day period
234 between August 2014 and April 2016. The grid, following the section, has variable horizontal resolution
235 with an upper limit of ~25km, and a uniform vertical resolution of 20m. These gridded data are primarily
236 based on continuous temperature, salinity and velocity measurements from twenty high-resolution
237 moorings (~15km apart) that were deployed in both boundaries of the Labrador Sea since August 2014
238 (see **Fig.1b** for location). The gridded data also incorporate many other observations in the region
239 including those from Argo, satellite altimetry and shipboard CTD stations.

240 In the boundaries covered by the moorings, moored property and velocity measurements are interpolated
241 onto the predefined grid mentioned above. Away from the moorings in the basin interior, the geostrophic

velocities are calculated from the two bounding dynamic height moorings by referencing to the time-mean surface velocities that are provided by satellite altimetry. In addition, a spatially-uniform compensation velocity is added at each 30-day period, yielding a 1.6 Sv southward net transport across the section to match the long-term observations across the Davis Strait[17]. Property fields in the basin interior down to 2000m are constructed via an objective analysis (OA) method[10,29,30]. The OA method used temperature and salinity from Argo profiles, OSNAP moorings, and World Ocean Atlas 2013 (WOA13) climatology. There are on average 99 Argo profiles in the Labrador Sea each month between 2014 and 2016. Below 2000m, data from the hydrographic sections during the summers of 2014 and 2016 are used.

The reader is referred to Lozier et al. (2019)[10] for a detailed description on the calculation method and the data products from OSNAP.

Reanalysis GloSea5

We also use data from the global ocean and sea ice reanalysis GloSea5[27,31], which uses the NEMO GO5 model with a nominal resolution of 0.25° and with 75 vertical layers[32] and the NEMOVAR v13 assimilation scheme[33]. The assimilated observations are: in-situ and satellite sea surface temperatures; sub-surface ocean profiles of temperature and salinity; sea ice concentration; and sea level anomalies. The experiment is described in more detail in Jackson et al. (2016)[27].

To show that the reanalysis data can adequately simulate the property field in the Labrador Sea, we compare the cross-sectional potential vorticity, temperature, salinity, density and velocity fields between GloSea5 and the OSNAP data during the observational period (Extended Data **Fig.1-3**). Overall, the magnitude and variability of MOC in the reanalysis compares fairly well with the observations.

There are two differences to note. First, the salinity gradient between the Labrador Current and the West Greenland Current is stronger in the reanalysis. Second, the maximum overturning in the reanalysis takes

place at a denser level (~27.80kg/m^3; Extended Data **Fig.3a**) compared to the observations (~27.70kg/m^3; **Fig.1a**), a difference that possibly attributable to a weaker stratification in the deep Labrador Sea in GloSea5.

Water mass definition in density space

Deep water masses in the Labrador Sea can be identified from property fields[12]. Along OSNAP West, LSW is identified by low salinity, relatively low temperature, low potential vorticity **(Fig.2)** and potential density (σ_θ, referenced to the surface), which is generally between 27.70 kg/m^3 and 27.80 kg/m^3. Below LSW, the Northeast Atlantic Deep Water (NEADW), with low temperature and high salinity, occupies the layer between 27.80 kg/m^3 and 27.89 kg/m^3. Finally, the layer below 27.89 kg/m^3 contains the Denmark Strait Overflow Water (DSOW), which has the lowest temperature and relatively low salinity. The water mass distribution shown here is very similar to those discussed in Yashayaev and Loder (2017)[12].

In this study, the water masses are defined only by σ_θ specified above because of its direct relationship with the stratification and potential energy. In addition, a definition in neutral density space does not show qualitative difference from that in σ_θ space.

Calculation of overturning in longitude-density space

In this study, the MOC is calculated as the maximum of the overturning streamfunction in σ_θ space,

$$MOC(t) = max\Psi(\sigma_\theta, t) = \max\left[-\int_{\sigma_{\theta max}}^{\sigma_\theta}\int_{x_e}^{x_w} v(x, \sigma_\theta, t)dxd\sigma_\theta\right], \quad [1]$$

where $v(x, \sigma_\theta, t)$ represents the transport component per unit length per unit density (unit: $(m^3 \cdot s^{-1})(m)^{-1}(kg \cdot m^{-3})^{-1}$) that is perpendicular to the section. A positive v indicates a flux into the basin (i.e. northwestward across OSNAP west). x_w denotes the westernmost position of the section, which is the Labrador Coast, and x_e denotes the easternmost position, which is the southwestern tip of Greenland.

The overturning streamfunction $\Psi(\sigma_\theta, t)$ is integrated from high density ($\sigma_{\theta max}$) to low density (σ_θ), which is different from the traditional calculation (from low density to high density). The latter method inevitably includes the southward flux of the lightest waters along the Labrador shelf that are not involved in the diapycnal transformation in the basin, leading to a smaller estimation of MOC (Extended Data **Fig.9**). Finally, we note that, in the Labrador Sea, the strength of the MOC in neutral density space is nearly identical to that in σ_θ space[10].

In **Fig.1a**, the 21-month mean $\overline{\Psi(\sigma_\theta, t)}$ is shown, whose maximum is 2.5Sv, reached at $27.70 kg/m^3$. This maximum is smaller than the mean of the monthly maximum streamfunctions, i.e. $\overline{max\Psi(\sigma_\theta, t)}$, which is 3.3Sv. This is because when averaging monthly streamfunctions, the level at which the maximum is reached is not taken into account[10]. As such, the mean streamfunction results in a weaker overturning.

Calculation of overturning in temperature-salinity space

To compute overturning in potential temperature-salinity (θ-S) space, we follow the approach in previous studies[34,35] by first computing volume transport in θ-S space,

$$v^*(\theta^*, S^*, t) = \frac{1}{\Delta\theta \Delta S} \iint \delta_{\Delta\theta} \delta_{\Delta S} v(x, z, t) dx dz, \quad [2]$$

where $\delta_{\Delta\theta}$ and $\delta_{\Delta S}$ are defined as discrete delta functions such that,

$$\delta_{\Delta\theta} = \begin{cases} 1, |\theta - \theta^*| \leq \Delta\theta/2 \\ 0, \quad elsewhere \end{cases}, \quad [3]$$

$$\delta_{\Delta S} = \begin{cases} 1, \quad |S - S^*| \leq \Delta S/2 \\ 0, \quad elsewhere \end{cases}. \quad [4]$$

As such, $v^*(\theta^*, S^*, t)$ is the transport over the bin area $\Delta\theta \times \Delta S$ at (θ^*, S^*), with units of $(m^3 \cdot s^{-1})(℃)^{-1}$. Following a series of sensitivity tests to assess which $\Delta\theta \times \Delta S$ best describes the

temperature/salinity structure in the Labrador Sea, $\Delta\theta$ is prescribed as 0.1°C and ΔS as 0.002. The overturning streamfunction with respect to temperature, $\Psi_\theta(\theta,t)$, and salinity space, $\Psi_S(S,t)$, can then be obtained by integrating $v^*(\theta^*,S^*,t)$ along isotherms and isohalines according to:

$$\Psi_\theta(\theta,t) = \int_{\theta_{max}}^{\theta} \int_{S_{min}}^{S_{max}} v^*(\theta^*,S^*,t) dS^* d\theta^*, \quad [5]$$

$$\Psi_S(S,t) = \int_{S_{max}}^{S} \int_{\theta_{min}}^{\theta_{max}} v^*(\theta^*,S^*,t) d\theta^* dS^*. \quad [6]$$

Here $\Psi_\theta(\theta,t)/\Psi_S(S,t)$ are both integrated from high to low values. Note that due to the high salinity contained in the NEADW layer, the salinity profile across OSNAP West is not monotonic with depth, different from density and temperature. As such, the strength of Ψ_S can be influenced by the transport in the salty NEADW layer. To exclude this influence and to keep the calculation consistent with that in temperature space, we calculate Ψ_S only with waters lighter than 27.80 kg/m^3. A test calculation of Ψ_S with all waters does not change any of our conclusions but only results in a stronger Ψ_S.

References

1. Wood, R. A., Keen, A. B., Mitchell, J. F. & Gregory, J. M. Changing spatial structure of the thermohaline circulation in response to atmospheric CO2 forcing in a climate model. *Nature* **399,** 572-575 (1999).
2. Rahmstorf, S. et al. Exceptional twentieth-century slowdown in Atlantic Ocean overturning circulation. *Nature Clim. change* **5,** 475-480 (2015).
3. Thornalley, D. J. et al. Anomalously weak Labrador Sea convection and Atlantic overturning during the past 150 years. *Nature* **556,** 227-230 (2018).
4. Straneo, F. On the connection between dense water formation, overturning, and poleward heat transport in a convective basin. *J. Phys. Oceanogr.* **36**, 1822-1840 (2006).

5. Pickart, R. S. & Spall, M. A. Impact of Labrador Sea convection on the North Atlantic meridional overturning circulation. *J. Phys. Oceanogr.* **37,** 2207-2227 (2007).
6. Rhein, M. et al. Labrador Sea Water: Pathways, CFC inventory, and formation rates. *J. Phys. Oceanogr.* **32**, 648-665 (2002).
7. Marsh, R. Recent variability of the North Atlantic thermohaline circulation inferred from surface heat and freshwater fluxes. *J. Clim.* **13**, 3239-3260 (2000).
8. Talley, L. D. Shallow, intermediate, and deep overturning components of the global heat budget. *J. Phys. Oceanogr.* **33**, 530-560 (2003).
9. Xu, X., Rhines, P. B., & Chassignet, E. P. On Mapping the Diapycnal Water Mass Transformation of the Upper North Atlantic Ocean. *J. Phys. Oceanogr.* **48**, 2233-2258 (2018).
10. Lozier, M. S. et al. A sea change in our view of overturning in the subpolar North Atlantic. *Science* **363(6426),** 516-521 (2019).
11. Lozier, M. S. et al. Overturning in the Subpolar North Atlantic Program: A new international ocean observing system. *Bull. Amer.* **98(4),** 737-752 (2017).
12. Yashayaev, I. & Loder, J. W. Further intensification of deep convection in the Labrador Sea in 2016. *Geophys. Res. Lett.* **44(3),** 1429-1438 (2017).
13. Lavender, K. L., Davis, R. E. & Owens, W. B. Mid-depth recirculation observed in the interior Labrador and Irminger seas by direct velocity measurements. *Nature* **407(6800),** 66-69 (2000).
14. Cuny, J., Rhines, P. B., Niiler, P. P. & Bacon, S. Labrador Sea boundary currents and the fate of the Irminger Sea Water. *J. Phys. Oceanogr.* **32(2),** 627-647 (2002).
15. Spall, M. A. Boundary currents and watermass transformation in marginal seas. *J. Phys. Oceanogr.* **34(5),** 1197-1213 (2004).
16. Katsman, C. A., Spall, M. A. & Pickart, R. S. Boundary current eddies and their role in the restratification of the Labrador Sea. *J. Phys. Oceanogr.* **34(9),** 1967-1983 (2004).
17. Curry, B., Lee, C. M. & Petrie, B. Volume, freshwater, and heat fluxes through Davis Strait, 2004–05. *J. Phys. Oceanogr.* **41(3),** 429-436 (2011).

18. Menary, M.B. et al. Exploring the impact of CMIP5 model biases on the simulation of North Atlantic decadal variability. *Geophys. Res. Lett.* **42**(14), 5926-5934 (2015).
19. Schneider, B., Latif, M. & Schmittner, A. Evaluation of different methods to assess model projections of the future evolution of the Atlantic meridional overturning circulation. *J. Clim.* **20(10),** 2121-2132 (2007).
20. Zhang, X. et al. Detection of human influence on twentieth-century precipitation trends. *Nature* **448(7152),** 461-465 (2007).
21. Heuzé, C. North Atlantic deep water formation and AMOC in CMIP5 models. *Ocean Sci.* **13(4),** 609-622 (2017).
22. Li, F. et al. Local and downstream relationships between Labrador Sea Water volume and North Atlantic meridional overturning circulation variability. *J. Clim.* **32(13),** 3883-3898 (2019).
23. Stocker, T. F. et al. IPCC Climate Change 2013: The Physical Science Basis.
24. Böning, C. W., Behrens, E., Biastoch, A., Getzlaff, K. & Bamber, J. L. Emerging impact of Greenland meltwater on deepwater formation in the North Atlantic Ocean. *Nature Geosci.* **9(7),** 523-527 (2016).
25. Jackson, L.C., Peterson, K.A., Roberts, C.D. & Wood, R.A. Recent slowing of Atlantic overturning circulation as a recovery from earlier strengthening. *Nature Geosci.* **9(7),** 518-522 (2016).
26. Chafik, L. & Rossby, T. Volume, Heat, and Freshwater Divergences in the Subpolar North Atlantic Suggest the Nordic Seas as Key to the State of the Meridional Overturning Circulation. *Geophys. Res. Lett.* **46**, 4799-4808 (2019).
27. Li, F., Lozier, M. S. & Johns, W. E. Calculating the meridional volume, heat, and freshwater transports from an observing system in the subpolar North Atlantic: Observing system simulation experiment. *J. Atmospheric Ocean. Technol.* **34(7),** 1483-1500 (2017).
28. Li, F. & Lozier, M. S. On the linkage between Labrador Sea Water volume and overturning circulation in the Labrador Sea: A case study on proxies. *J. Clim.* **31(13),** 5225-5241 (2018).

29. Blockley, E. W. et al. Recent development of the Met Office operational ocean forecasting system: an overview and assessment of the new Global FOAM forecasts. *Geoscientific Model Development* **7(6),** 2613-2638 (2014).
30. Megann, A. P. et al. GO 5.0: The joint NERC-Met Office NEMO global ocean model for use in coupled and forced applications. *Geotechnical Model Development* **7(3),** 1069-1092 (2014).
31. Waters, J. et al. Implementing a variational data assimilation system in an operational 1/4 degree global ocean model. *Q. J. Roy. Meteor. Soc.* **141(687),** 333-349 (2015).
32. Zika, J. D., England, M. H. & Sijp, W. P. The ocean circulation in thermohaline coordinates. *J. Phys. Oceanogr.* **42(5),** 708-724 (2012).
33. Xu, X., Rhines, P. B. & Chassignet, E. P. Temperature–salinity structure of the North Atlantic circulation and associated heat and freshwater transports. *J. Clim.* **29(21),** 7723-7742 (2016).
34. Good, S. A., Martin M. J. & Rayner N. A. EN4: quality controlled ocean temperature and salinity profiles and monthly objective analyses with uncertainty estimates, *J. Geophys. Res.: Oceans* **118**, 6704-6716 (2013).

Corresponding Author

Correspondence and requests for materials should be addressed to Sijia Zou at szou@whoi.edu.

Acknowledgements

S. Zou, M.S. Lozier and F. Li gratefully acknowledge the Physical Oceanography Program of the U.S. National Science Foundation (fund code: 3331843). R. Abernathey acknowledges support from NSF award OCE 1553593. L. Jackson is funded by the Copernicus Marine Environment Monitoring Service (CMEMS: 23-GLO-RAN). The authors would like to acknowledge the work of K.A. Peterson in creating the GloSea5 reanalysis.

Data availability

OSNAP data were collected and made freely available by the OSNAP project and all the national programs that contribute to it (www.o-snap.org). Data from the full OSNAP array for the first 21 months (31-Jul-2014 to 20-Apr-2016) have been used to produce the 30-day mean time series across the whole section, as well as the gridded property fields. The DOI for this derived data is 10.7924/r4z60gf0f. Data from GloSea5 (re-gridded to 1x1 degree) is available from http://marine.copernicus.eu/services-portfolio/access-to-products/ under product name GLOBAL_REANALYSIS_PHY_001_026. EN4.2.1 data used in **Extended Data Fig.4,6** are downloaded from https://www.metoffice.gov.uk/hadobs/en4/.

Code availability

The code used to generate MOC and transport in temperature and salinity space can be accessed on request to S.Z.

Author contributions

S. Z., M.S.L. and F.L. led the data analysis. F.L. conducted the MOC calculation. R.A. proposed and formulated the calculation of overturning in temperature and salinity space. L.J. provided the GloSea5 data and assisted with the calculation of MOC. All authors contributed to results interpretation and manuscript writing.

Extended data

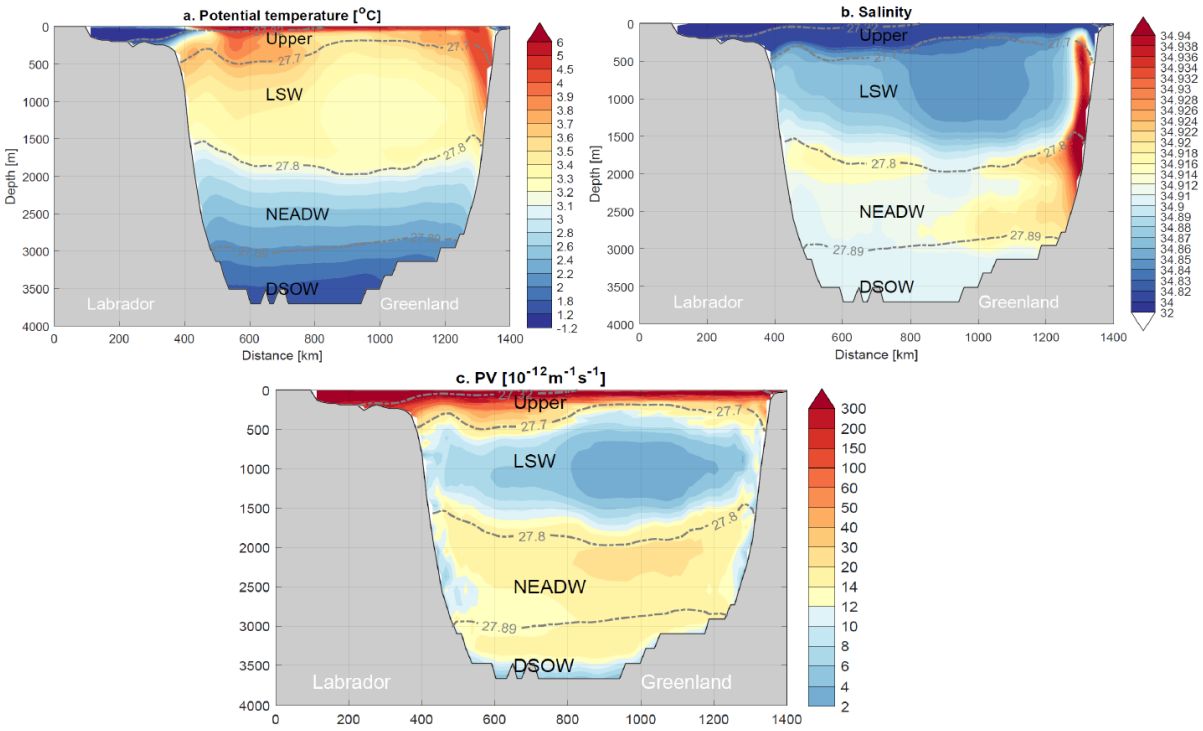

418

419 **Extended Data Fig.1: Simulated mean property distribution in GloSea5. (a)** Mean potential
420 temperature averaged between August 2014 and April 2016 along simulated OSNAP West section. **(b)**
421 Mean salinity from the same source. **(c)** Mean PV ($\times 10^{-12} m^{-1} s^{-1}$) from the same source. The
422 simulated OSNAP West section is created using model grid points that minimize the distance from the
423 grid locations to the observational locations. Temperature, salinity and PV are then extracted along the
424 section. Note that the section definition allows for an accurate calculation of the transport on the model
425 grid.

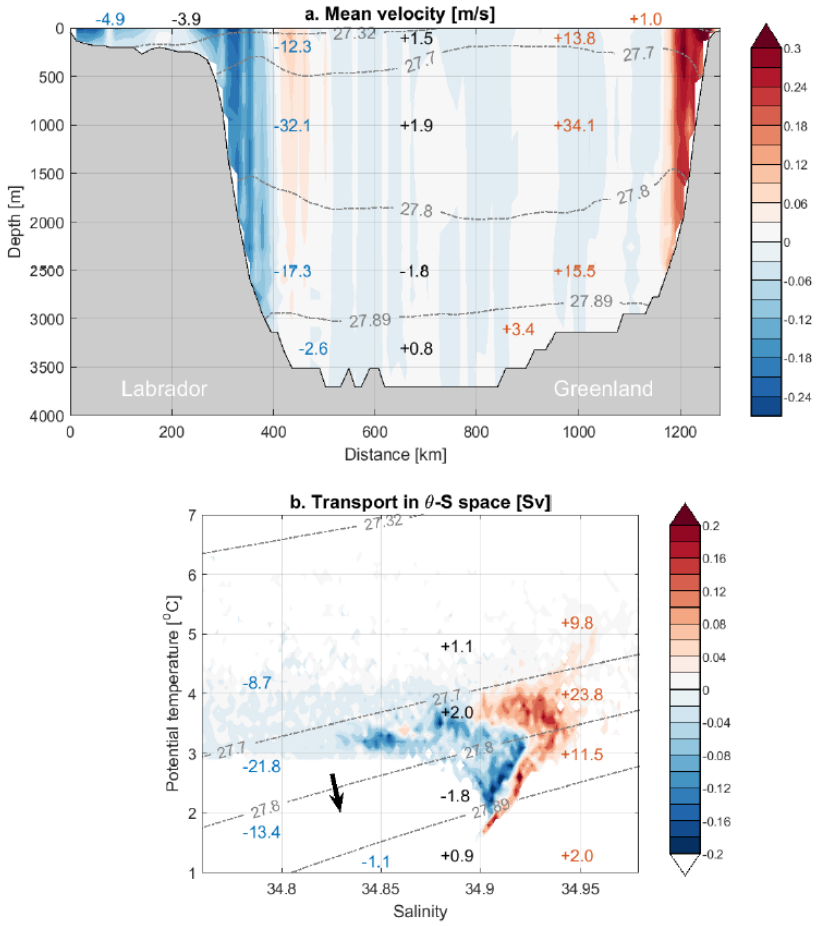

426

427 **Extended Data Fig.2**: **Simulated mean circulation in GloSea5. (a)** The mean velocity perpendicular to
428 the simulated OSNAP West section during August 2014 and April 2016. Positive (negative) velocities
429 indicate flow into (out of) the basin. Mean volume flux in each density class is labeled, similar to that in
430 **Fig.1b**. Note that the along-isopycnal transport in each layer is stronger in GloSea5 compared to the
431 observations (**Fig.1b**). This is because that when integrating the total positive/negative transport across
432 the section, the recirculation branches in the basin interior are also included. **(b)** Mean volume flux in θ-S
433 space from the reanalysis. Black arrow indicates direction of the diapycnal transformation.

434

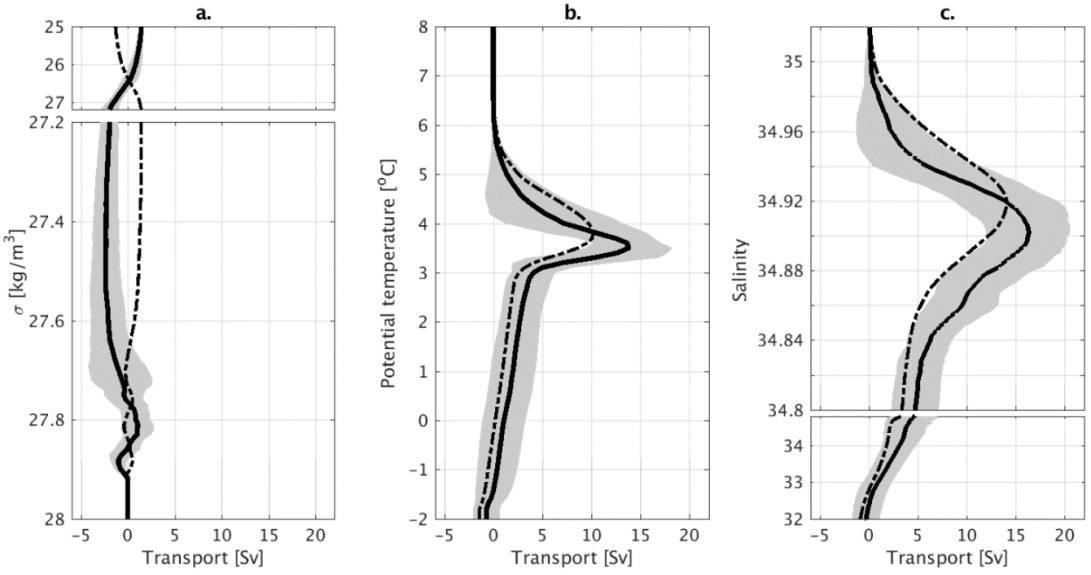

435

436 **Extended Data Fig.3: Simulated mean overturning streamfunction in GloSea5. (a)** The mean
437 overturning streamfunction in density space during August 2014 - April 2016 (solid black), with monthly
438 SD shaded in gray. Dashed curve indicates the overturning streamfunction averaged over the entire
439 temporal domain from the reanalysis (i.e. 1993-2017). **(b)** Similar to **(a)**, but in θ space. **(c)** Similar to **(a)**,
440 but in S space.

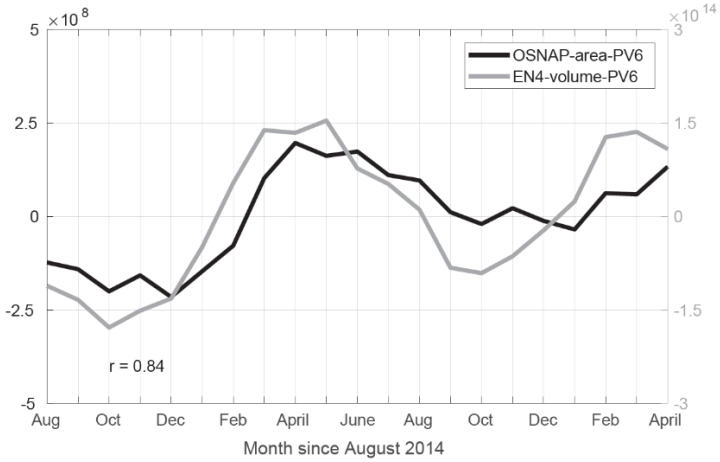

441

442 **Extended Data Fig.4: Observed monthly variability of LSW volume.** Monthly time series of the total
443 area (unit: m^2) with low potential vorticity (PV≤$6\times10^{-12}m^{-1}s^{-1}$) across OSNAP West from
444 observations (black), and the total volume (unit: m^3) with low PV in the entire Labrador Basin (gray)

445 from the Met Office Hadley Centre observational datasets EN4.2.1[36]. Plotted are the anomalies relative to
446 the 21-month mean.

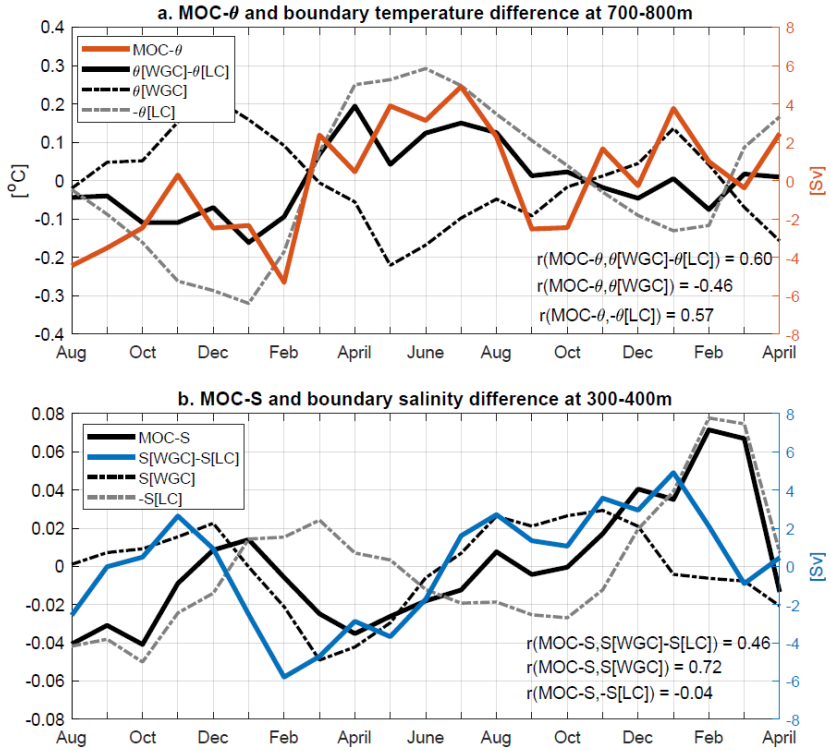

447

448 **Extended Data Fig.5: Observed relationship between MOC_θ (MOC_S) and temperature (salinity)**
449 **distribution. (a)** Observed monthly anomalies of MOC_θ (orange) since August 2014 and potential
450 temperature difference between the WGC and the LC (i.e. $\theta[WGC] - \theta[LC]$) at 700-800 m (solid black),
451 the depths at which the correlation between the two time series is the strongest. The temperature
452 anomalies for the WGC (i.e. $\theta[WGC]$) are plotted in dashed black and the negative temperature anomalies
453 for the LC (i.e. $-\theta[LC]$) are shown in dashed gray. **(b)** Similar to **(a)**, but for MOC_S and salinity
454 anomalies in the boundary current.

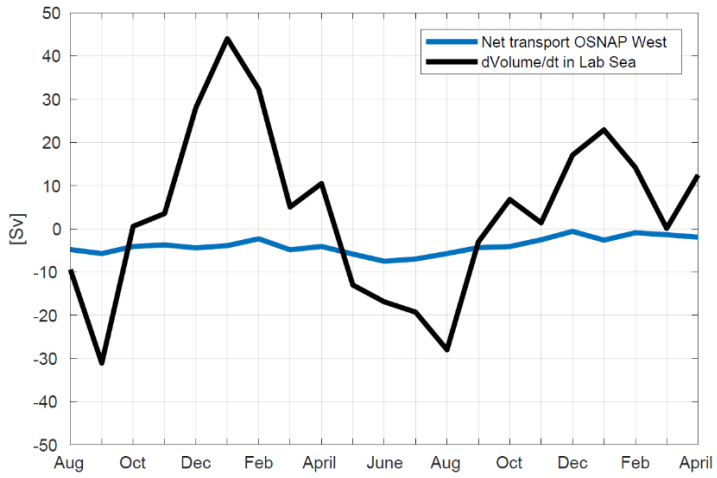

455

456 **Extended Data Fig.6: Strong monthly LSW layer volume variability.** Plotted in black is the LSW

457 layer (27.70-27.80kg/m^3) volume variability within the Labrador Sea (northwest of OSNAP West) since

458 August 2014, which is derived from EN4.2.1[36]. Observed monthly transport in the LSW layer across

459 OSNAP West is plotted in blue. The variability between the two time series is similar (r=0.61), but the

460 magnitude differs significantly.

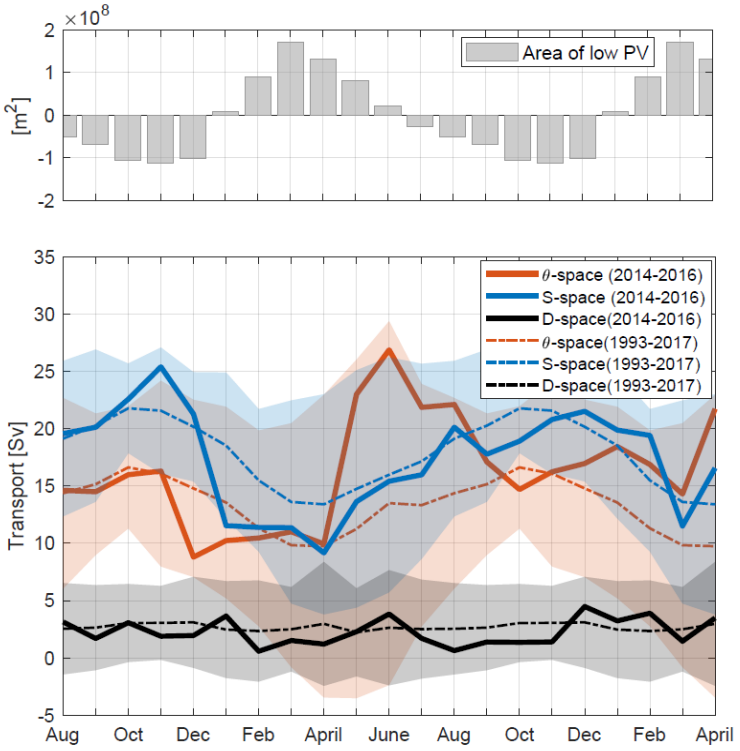

461

Extended Data Fig.7: Simulated monthly LSW volume and overturning transports in GloSea5. Climatological monthly time series of newly-formed LSW volume (gray bars), MOC_θ (dashed orange), MOC_S (dashed blue), and MOC_σ (dashed black) from GloSea5 during 1993-2017. Shaded areas represent 2×standard deviation of the annually varying transport for each month. The simulated transport time series during the OSNAP time period (August 2014 – April 2016) are plotted in solid colored lines.

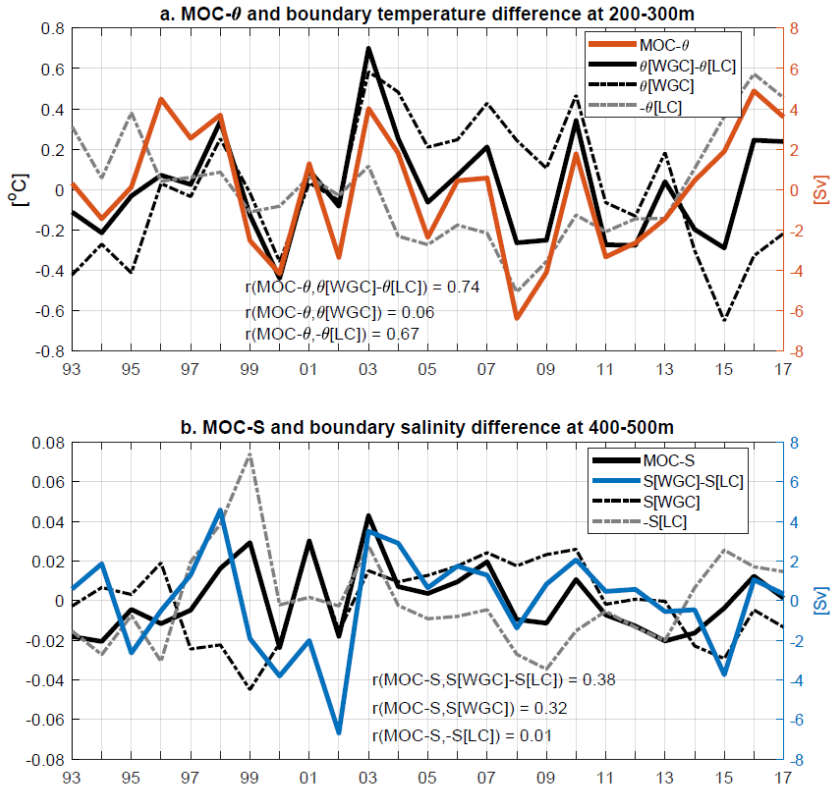

Extended Data Fig.8: **Relationship between interannual MOC_θ (MOC_S) and temperature (salinity) distribution in GloSea5.** **(a)** Simulated annual anomalies of MOC_θ (orange) and the temperature difference between the WGC and the LC (i.e. $\theta[WGC] - \theta[LC]$) at 200-300m (solid black). The depths between 200-300m are where the maximum correlation between MOC_θ and temperature difference is reached. The temperature anomalies for the WGC alone (i.e. $\theta[WGC]$) are plotted in dashed black and the minus temperature anomalies for the LC (i.e. $-\theta[LC]$) are plotted in dashed gray. **(b)** Similar to **(a)**, but for MOC_S and salinity anomalies in the boundary current.

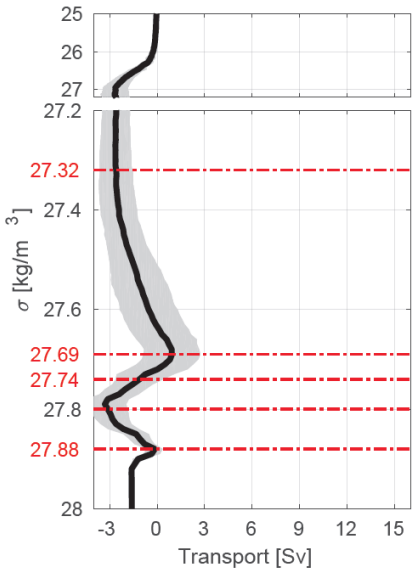

475

476 **Extended Data Fig.9: Observed overturning streamfunction with the traditional calculation.** The
477 21-month mean overturning streamfunction integrated from low density to high density (solid black),
478 with monthly standard deviation shaded in gray. The MOC with this calculation is 1.4±1.7Sv (see
479 **Methods**).